Polarized Alkali-Metal Vapor with Minute-Long Transverse Spin-Relaxation Time

M. V. Balabas,[1] T. Karaulanov,[2] M. P. Ledbetter,[2,*] and D. Budker[2,3]

[1]S. I. Vavilov State Optical Institute, St. Petersburg, 199034 Russia
[2]Department of Physics, University of California at Berkeley, Berkeley, California 94720-7300, USA
[3]Nuclear Science Division, Lawrence Berkeley National Laboratory, Berkeley California 94720, USA

(Received 7 May 2010; published 12 August 2010)

We demonstrate lifetimes of Zeeman populations and coherences in excess of 60 sec in alkali-metal vapor cells with inner walls coated with an alkene material. This represents 2 orders of magnitude improvement over the best paraffin coatings. We explore the temperature dependence of cells coated with this material and investigate spin-exchange relaxation-free magnetometry in a room-temperature environment, a regime previously inaccessible with conventional coating materials.

DOI: 10.1103/PhysRevLett.105.070801 PACS numbers: 07.55.Ge, 32.80.Xx, 42.65.−k

Long-lived ground-state polarization in atomic vapor cells forms the basis for atomic clocks [1–3], magnetometers [4,5], quantum memory [6], spin-squeezing and quantum nondemolition measurements [7,8], and precision measurements of fundamental symmetries [9]. One method for achieving long coherence times is to coat the walls of a cell with an antirelaxation film such as paraffin [10,11] or octadecyltrichlorosilane [12]. Conventional paraffin coatings are formed from long-chain alkane molecules, supporting approximately 10^4 atom-wall collisions before depolarizing the alkali-metal spins. In this Letter we report on the remarkable antirelaxation properties of a new, alkene based, coating. With proper experimental arrangements, we realize coherence lifetimes on the order of 1 min in a 3 cm diameter cell, corresponding to about 10^6 polarization preserving bounces. To the best of our knowledge, this corresponds to the narrowest electron paramagnetic resonance ever observed.

A key to such long lifetimes is to work in magnetic fields such that the Larmor precession frequency is small compared to the spin-exchange rate $1/T_{\mathrm{ex}} = n\sigma_{\mathrm{ex}}\upsilon$ (n is the number density, σ_{ex} is the spin-exchange cross section, and υ is the mean relative thermal velocity), and to optically pump the alkali-metal vapor with circularly polarized light. Under these conditions, the alkali-metal spins precess at a modified rate, and spin-exchange relaxation is quadratic in the magnetic field, and vanishes at zero magnetic field, the so-called spin-exchange relaxation-free (SERF) regime [13,14]. SERF magnetometers presently hold the record for magnetic-field sensitivity of any device [15,16], but usually require operation at temperatures in excess of 150 °C. The alkene coating described here enables operation of such a magnetometer in a room-temperature environment, expanding its useful range of application, especially where low power consumption is important. We present an experimental and theoretical investigation of a room-temperature SERF magnetometer.

Exchange of atoms between the bulb and the stem with the Rb reservoir (Fig. 1) can produce rapid relaxation. This can be avoided by employing a ''lockable stem'' [17] which provides a coated barrier to reduce the rate of exchange between the bulb and the stem. Finally, gradients of the magnetic field are another source of relaxation, so care must be taken to minimize them.

Reference [18] reports lifetimes of about 3 sec in alkali-metal vapor cells coated with the alkene 1-nonadecene ($CH_2 - CH(CH_2)_{16} - CH_2$). To further investigate alkene based coatings, we prepared three Rb-vapor cells with lockable stems. Cells C1 and C2 had natural-abundance Rb and nonideal locks, cell C3 had ^{87}Rb and a ''precision ground'' lock. The initial material for the coating preparation was Alpha Olefin Fraction C20-24 from Chevron Phillips (CAS Number 93924-10-8). A light fraction of the material was removed through vacuum distillation at 80 °C and the remains were used as the coating material. Coatings were prepared with the procedure described in Refs. [4,19], except the temperature was 175 °C instead of 220 °C. After preparation, the cells were cured at 70 °C for several hours. Cell C1 had a polarization lifetime of 60 sec, while cells C2 and C3 had polarization lifetimes of about

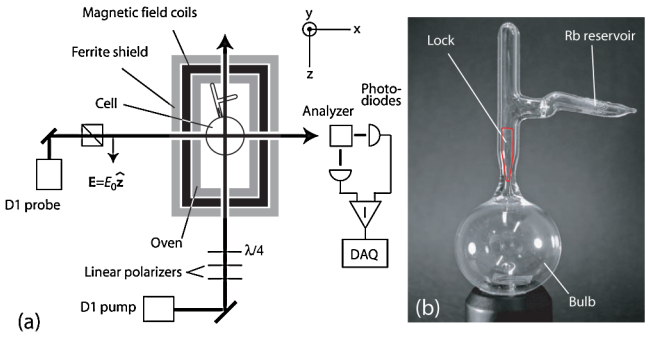

FIG. 1 (color online). Experimental setup: (a) Four mu-metal shields (not shown) surround the ferrite shield. The ferrite shield is a cylinder, 15.2 cm long and 11.4 cm in diameter (inner dimensions) with 1.3 cm thick walls. A set of coils provides control over the magnetic fields. The oven was temperature controlled by running ac current through twisted-pair copper wire. (b) Photo of the coated cell.

15 sec. The measurements presented here were obtained with cell C1.

The experimental setup is shown in Fig. 1(a). The coated cell was placed inside four layers of mu metal and one layer of ferrite [16] shielding. The alkali-metal spins were optically pumped by circularly polarized light propagating in the z direction, resonant with the $F = 2 \rightarrow F'$ D1 transitions of ^{85}Rb. Pump power ranged from 0–2 μW. Spin precession was monitored via optical rotation of linearly polarized probe light, propagating in the x direction, tuned about 1.5 GHz to the blue of the $F = 3 \rightarrow F'$ D1 transitions of ^{85}Rb. Optical rotation, scaling roughly as the inverse of detuning, was dominated by ^{85}Rb, with smaller contribution from ^{87}Rb. Typical probe power was ≈ 2 μW, although much higher probe power could be used without incurring substantial additional broadening since the probe was tuned far off resonance. Most of the measurements were performed at 30 °C where the Rb-vapor density was $n \approx 1.5 \times 10^{10}$ cm^{-3}, determined by transmission of a weak probe beam. The spin-exchange cross section for Rb is $\sigma_{\mathrm{ex}} = 1.9 \times 10^{-14}$ cm^{-2} [20], yielding a spin-exchange rate $1/T_{\mathrm{ex}} = n\sigma_{\mathrm{ex}}v = 11.1$ s^{-1} at 30 °C. The orientation of the cell could be manipulated from outside the magnetic shields so that the lock could be opened and closed without opening the shields. With the lock open, polarization lifetimes were much shorter than with the lock closed, approximately 3 sec. Geometry dictated that the stem and locking bullet were nearly horizontal, producing a lock of variable quality: the longitudinal relaxation time varied by as much as a factor of 4 from run to run.

Longitudinal (with respect to magnetic field) relaxation was measured by first applying a field parallel to the pump beam, adiabatically rotating the field into the direction of the probe beam, and then monitoring optical rotation of the probe as the longitudinal polarization decayed. To investigate transverse relaxation, we observed the transient response of the alkali-metal spins to a nonadiabatic change in the magnetic field, either by (i) pumping the spins in zero magnetic field and applying a step in B_y, or (ii) by pumping the spins in a finite bias magnetic field B_z and then applying a short pulse of magnetic-field B_x. We also made high-field (10–20 G) measurements of the longitudinal relaxation time using an apparatus similar to that in Ref. [21].

Figure 2 shows optical rotation of the probe due to longitudinal (a) and transverse (b) polarization when the cell was performing optimally. The decay of longitudinal polarization is well described by two exponentials with fast and slow time constants $T_{1f} = 8$ s and $T_{1s} = 53$ s, respectively. Such biexponential decays arise from several competing processes of electron spin-destruction collisions with the cell walls, residual relaxation due to collisions with the reservoir, and alkali-metal–alkali-metal spin-exchange collisions [21].

Figure 2(b) shows the transient response to a step in the magnetic-field $B_y \approx 0.2$ μG after pumping at zero magnetic field. In the absence of spin-exchange collisions, the Larmor precession frequency would be about 0.1 and 0.15 Hz for ^{85}Rb and ^{87}Rb, respectively, roughly 100 times smaller than the rate of spin-exchange collisions, well within the SERF regime. Under these conditions, both hyperfine manifolds of the two isotopes "lock" together, precessing with a modified frequency and decaying back to equilibrium with fast and slow decays characterized by lifetimes T_{2f} and T_{2s}. For the data shown in Fig. 2(b), $T_{2f} = 13$ s and $T_{2s} = 77$ s. We note that low-field values of T_{1s} and T_{2s} were somewhat shorter in subsequent measurements, around 25–35 s. Under these conditions, the fast relaxation was not apparent, and curves were fit with a single decay time, T_{1s} or T_{2s}. With the stem oriented vertically, high-field measurements of T_{1s} were consistently long over the course of several months, in the range of 40–50 sec. Hence, we suspect that minute-long lifetimes in low field were difficult to reproduce because of the variable quality of the locking stem in the nearly horizontal position.

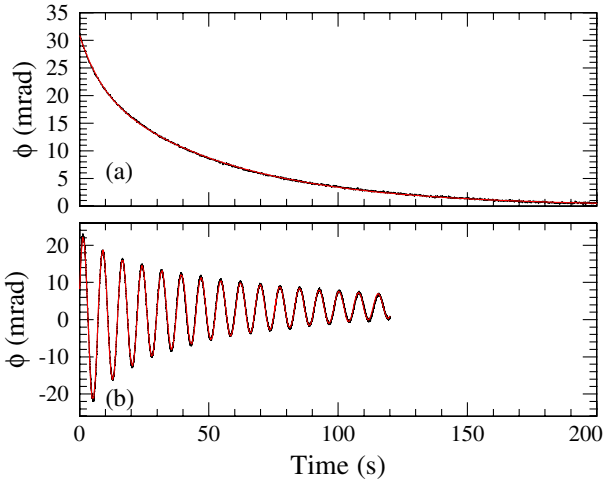

FIG. 2 (color online). (a) Decay of longitudinal polarization. The red trace overlaying the data is a fit to two decaying exponentials, with fast and slow decay times of 8 and 53 seconds, respectively. (b) Response of alkali-metal spin polarization to a transient of the magnetic field. The fast and slow decay times are 13 and 77 sec.

Wall coatings are characterized by the number of bounces a polarized atom can survive before becoming depolarized. By assuming the usual cosine distribution of atoms leaving the wall, one can show that the mean time between wall collisions for a spherical cell of radius R is $\tau_c = 4R/3\bar{v}$, where $\bar{v}$ is the mean velocity. For $R = 1.5$ cm, and taking the maximum lifetime $T_{2s} = 77$ s, we find that the coating supports approximately $T_{2s}/\tau_c \approx 10^6$ collisions.

To further characterize the coating, Fig. 3 shows the temperature dependence of the alkali-metal density and longitudinal relaxation rate. In acquiring these data, we let the oven and cell equilibrate for several hours at each temperature before measuring the density and lifetime. The

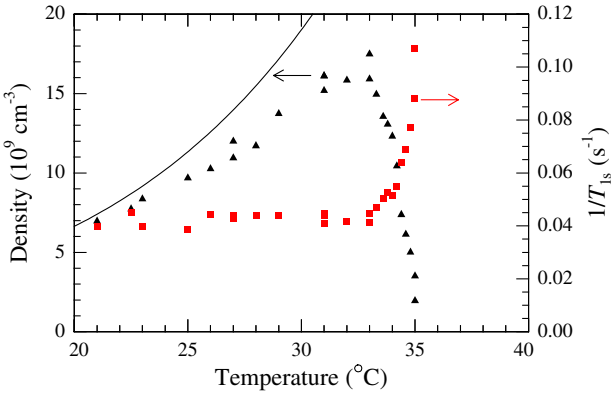

FIG. 3 (color online). Rb-vapor density (triangles) and relaxation rate (squares) as a function of temperature. Density loosely follows that of a saturated vapor (solid curve) until it drops rapidly at the melting point of the coating ≈ 33 °C, accompanied by an increase in the relaxation rate.

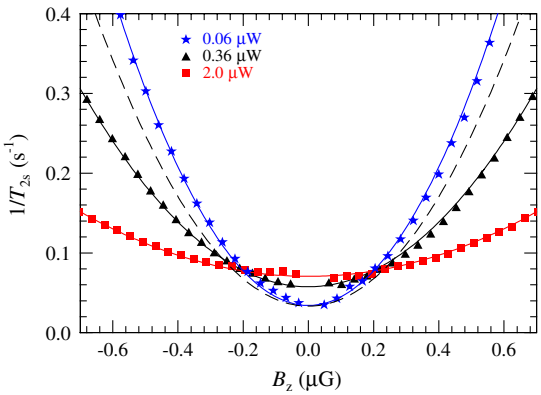

FIG. 4 (color online). Transverse relaxation rate as a function of magnetic field for several values of the pump power. The smooth curves overlaying the data are fits described in the text. The dashed curve is the relaxation rate in the low-polarization limit given by Eq. (1) for nuclear spin $I = 5/2$.

lock was closed the entire time. We see a sharp drop in density and an increase in relaxation rate as we pass through the melting transition of the coating at ≈33 °C. This behavior was repeatable and without significant hysteresis, as data points were acquired nonsequentially. The solid curve represents the expected density for a saturated vapor [22], which begins to deviate from the measured density at relatively low temperature. We suspect that the behavior shown in Fig. 3, may be related to an increase in the adsorption energy above the melting point. Alternatively, the rate of Rb atoms diffusing into the coating may increase above the melting point.

We now turn to a more detailed discussion of the effects of spin exchange in a low-density vapor in the limit of rapid spin exchange, $\omega_0 = g_s \mu_B B/(2I+1)\hbar \ll 1/T_{ex}$, where I is the nuclear spin, g_s is the Landé factor for the electron, and μ_B is the Bohr magneton. For a single isotope, spin-exchange relaxation of a low-polarization spin-temperature distribution is given by [23]

$$\Gamma_{SE} = \omega_0^2 T_{ex} \frac{(2I+1)(1-C^{-2})}{2C}, \qquad (1)$$

where the parameter $C = [(2I+1)^2 + 2]/[3(2I+1)]$ relates the modified precession frequency to the free-precession frequency in the absence of spin exchange, $\omega = \omega_0/C$.

The magnetic-field dependence of the transverse relaxation rate, $1/T_{2s}$, for several pump powers is shown in Fig. 4. In acquiring these data, transverse coherences were produced by applying a short (0.2 s) pulse of magnetic field in the x direction in the presence of a static field B_z. The solid curves overlaying the data are fits to $A + A_{SE}B_z^2$, where A represents relaxation due to wall collisions, pump light, and gradients, and A_{SE} represents the contribution to broadening from spin-exchange collisions. At low magnetic field, increasing pump power produces power broadening, however, at higher magnetic fields, high pump power reduces spin-exchange relaxation by preferentially populating the stretched state, which is immune to spin-exchange relaxation [24]. The dashed curve in Fig. 4 represents the limit given by Eq. (1) for a vapor of pure ^{85}Rb ($I = 5/2$) with T_{ex} determined by transmission measurements of the density. Equation (1) appears close to accounting for relaxation at low light power, however there is some discrepancy, presumably due to the presence of two isotopes.

The gyromagnetic ratio also varies significantly with pump power. In order to compare with theoretical calculations (see below) it is convenient to plot the measured spin-exchange broadening A_{SE} as a function of the effective gyromagnetic ratio γ (Fig. 5, triangles). It is interesting to note that there is a linear relationship between these two parameters, as indicated by the linear fit overlaying the data. It is also worth noting that, spin-exchange broadening approaches an asymptotic value of about 0.2 s$^{-1}/\mu$G^2 at

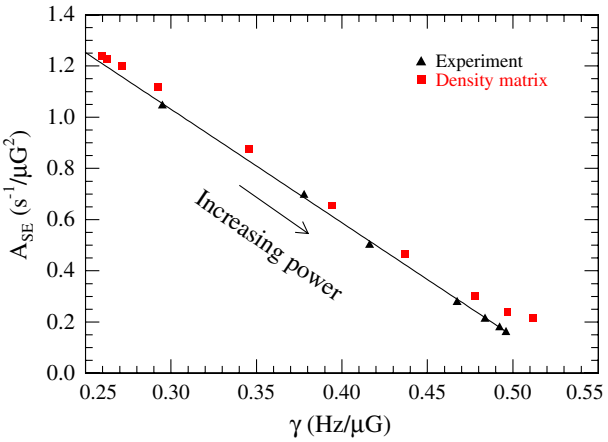

FIG. 5 (color online). Triangles show experimental measurements of spin-exchange broadening A_{SE} vs the effective gyromagnetic ratio γ for pump power ranging from 0.06 μW to 2 μW. The straight line overlaying the data is a linear fit. Squares show the results of density matrix calculations.

high power due to the presence of two isotopes, as can be seen by the clustering of data points at high light power, despite the increasing size of light-power steps. In an isotopically pure vapor, high pump power would more effectively reduce spin-exchange relaxation, similar to the light narrowing observed in Ref. [24].

To further investigate the effects of spin-exchange collisions, we performed numerical simulations following the approach used in Refs. [25,26]. The contributions to evolution of the ground-state density matrix ρ_j for isotope j due to hyperfine splitting, Zeeman splitting, optical pumping, spin-destruction, and spin-exchange are, respectively,

$$\frac{d\rho_j}{dt} = \frac{a_j}{i\hbar}[\mathbf{I}_j \cdot \mathbf{S}_j, \rho_j] + \frac{g_s \mu_B}{i\hbar}[\mathbf{B} \cdot \mathbf{S}_j, \rho_j] + R_j[\phi_j(1 + 2\hat{\mathbf{z}} \cdot \mathbf{S}_j) - \rho_j] + \frac{\phi_j - \rho_j}{T_{\mathrm{sd}}} + \sum_k \frac{\phi_j(1 + 4\langle \mathbf{S}_k \rangle \cdot \mathbf{S}_j) - \rho_j}{T_{\mathrm{ex},jk}}. \quad (2)$$

Here a_j is the hyperfine constant, $\mathbf{I}_j$ is the nuclear spin, R_j is the optical pumping rate for isotope j (0 for ^{87}Rb since the pump light is resonant only with ^{85}Rb transitions), and $\phi_j = \rho_j/4 + \mathbf{S}_j \cdot \rho_j \mathbf{S}_j$ is the purely nuclear part of the density matrix. The spin-destruction rate T_{sd} is determined from measurements of T_1, and the spin-exchange rates $1/T_{\mathrm{ex},jk} = n\eta_k\sigma_{\mathrm{ex}}$ (η_k is the natural abundance of isotope k) are determined by the measured alkali-metal density and the known cross sections. The transient response to a pulse of magnetic field in the y direction and subsequent precession around a static field in the z direction is determined by numerically integrating Eq. (2), starting from a spin-temperature distribution along the z axis. We extract the x component of electron spin polarization, weighted by isotopic abundance, $\langle S_x \rangle = \eta_{85}\langle S_{x,85} \rangle + \eta_{87}\langle S_{x,87} \rangle$, a reasonable approximation of the experimental observable, and fit this to a decaying sinusoid. The squares in Fig. 5 show the results of simulations. Experiment and simulation are in good agreement for low light power, although there is some small systematic offset, which we attribute to uncertainty in the alkali-metal vapor density. At higher light power, the simulation deviates from experiment, presumably because the optical pumping term in Eq. (2) is correct in the limit of unresolved hyperfine structure, and therefore cannot account for hyperfine pumping present in the experiment.

In conclusion, we have demonstrated that an alkene coating can support up to 10^6 alkali-metal-wall collisions before depolarizing the alkali-metal spins, representing an improvement by nearly a factor of 100 over traditional alkane coatings. We demonstrate that cells employing such a coating can enable operation of a SERF magnetometer in a low-density, room-temperature environment, a regime inaccessible to buffer-gas cells or cells with conventional paraffin coatings. We have investigated the behavior of such a magnetometer employing two alkali-metal isotopes, potentially of interest in comagnetometry schemes. Future work will investigate linewidths and shifts of hyperfine transitions in alkene coated cells in the context of atomic clocks. Finally, we mention that, in conjunction with light-narrowing techniques [24] to reduce spin-exchange relaxation, alkene coated cells with a single Rb isotope may afford sufficiently resolved lines to reduce systematic ''heading errors'' associated with the nonlinear Zeeman effect [27] in the range of geophysical fields.

The authors appreciate useful discussions with S. Bernasek and V. M. Acosta. This work was supported by the ONR MURI and NGA NURI programs and by the NSF.

*ledbetter@berkeley.edu

[1] H. G. Robinson and C. E. Johnson, Appl. Phys. Lett. **40**, 771 (1982).
[2] A. Risley, S. Jarvis, and J. Vanier, J. Appl. Phys. **51**, 4571 (1980).
[3] C. Rahman and H. G. Robinson, IEEE J. Quantum Electron. **23**, 452 (1987).
[4] E. B. Alexandrov *et al.*, Phys. Rev. A **66**, 042903 (2002).
[5] D. Budker and M. V. Romalis, Nature Phys. **3**, 227 (2007).
[6] B. Julsgaard *et al.*, Nature (London) **432**, 482 (2004).
[7] A. Kuzmich, L. Mandel, and N. P. Bigelow, Phys. Rev. Lett. **85**, 1594 (2000).
[8] W. Wasilewski *et al.*, Phys. Rev. Lett. **104**, 133601 (2010).
[9] W. C. Griffith *et al.*, Phys. Rev. Lett. **102**, 101601 (2009).
[10] H. G. Robinson, E. S. Ensberg, and H. G. Dehmelt, Bull. Am. Phys. Soc. **3**, 9 (1958).
[11] M. A. Bouchiat and J. Brossel, Phys. Rev. **147**, 41 (1966).
[12] S. J. Seltzer, P. J. Meares, and M. V. Romalis, Phys. Rev. A **75**, 051407(R) (2007).
[13] J. C. Allred, R. N. Lyman, T. W. Kornack, and M. V. Romalis, Phys. Rev. Lett. **89**, 130801 (2002).
[14] W. Happer and H. Tang, Phys. Rev. Lett. **31**, 273 (1973).
[15] I. K. Kominis, T. W. Kornack, J. C. Allred, and M. V. Romalis, Nature (London) **422**, 596 (2003).
[16] T. W. Kornack *et al.*, Appl. Phys. Lett. **90**, 223501 (2007).
[17] T. Karaulanov *et al.*, Phys. Rev. A **79**, 012902 (2009).
[18] M. V. Balabas *et al.*, Opt. Express **18**, 5825 (2010).
[19] M. V. Balabas, Ph.D. thesis, Vavilov State Optical Institute, 1995.
[20] D. K. Walter, W. M. Griffith, and W. Happer, Phys. Rev. Lett. **88**, 093004 (2002).
[21] M. T. Graf *et al.*, Phys. Rev. A **72**, 023401 (2005).
[22] *CRC Handbook of Chemistry and Physics* (CRC Press, Cleveland, 1993), 74th ed., p. 4124.
[23] W. Happer and A. C. Tam, Phys. Rev. A **16**, 1877 (1977).
[24] S. Appelt, A. B. Baranga, A. R. Young, and W. Happer, Phys. Rev. A **59**, 2078 (1999).
[25] S. Appelt *et al.*, Phys. Rev. A **58**, 1412 (1998).
[26] I. M. Savukov and M. V. Romalis, Phys. Rev. A **71**, 023405 (2005).
[27] E. B. Alexandrov, Phys. Scr. **t105**, 27 (2003).